Atmos. Chem. Phys. Discuss., https://doi.org/10.5194/acp-2018-38
Manuscript under review for journal Atmos. Chem. Phys.
Discussion started: 6 February 2018


Atmospheric Chemistry and Physics Discussions

# Scale dependence of cirrus heterogeneity effects. Part II: MODIS VNIR and SWIR channels

Thomas Fauchez[1,2], Steven Platnick[2], Tamás Várnai[3,2], Kerry Meyer[2], Céline Cornet[4], and Frédéric Szczap[5]

[1]Universities Space Research Association (USRA), Columbia, MD, USA
[2]NASA Goddard Space Flight Center, Greenbelt, MD, USA
[3]University of Maryland Baltimore County: Joint Center for Earth Systems Technology and the Department of Physics , Baltimore, MD, USA
[4]Laboratoire d'Optique Atmosphèrique, UMR 8518, Université Lille 1, Villeneuve d'Ascq, France
[5]Laboratoire de Météorologie Physique, UMR 6016, Université Blaise Pascal, Clermont Ferrand, France

*Correspondence to:* Thomas Fauchez (thomas.j.fauchez@nasa.gov)

**Abstract.** The understanding of the radiative role of clouds is crucial. Ice clouds such as cirrus have, on average, a significant positive radiative effect, while in some conditions it may be negative. However, many uncertainties remain on the role of this type of clouds on Earth's radiative budget and in a changing climate. Global satellite observations are particularly well suited to monitor clouds, retrieve their characteristics and infer their radiative impact. To retrieve ice cloud properties (optical thickness and ice crystal effective size), current operational algorithms assume that each pixel of the observed scene is plane-parallel and homogeneous, and that there is no radiative connection between neighboring pixels. This retrieval representation is far from the reality, where the radiative transfer is 3D, leading to the plane parallel and homogeneous bias (PPHB) and the independent pixel approximation bias (IPAB) impacting both the estimation of top of the atmosphere (TOA) radiation and retrievals. An important factor that constrains the impact of these assumptions is the sensor spatial resolution. High spatial resolution pixels can better represent cloud variability (low PPHB) though the radiative path through the cloud can involve many pixels (high IPAB). In contrast, low spatial resolution pixels poorly represent the cloud variability (high PPHB) but the radiation is better contained within the pixel field of view (low IPAB). In addition, the solar and viewing geometry (as well as cloud optical properties) can modulate the magnitude of the PPHB and IPAB. In this Part II of our study, we have simulated TOA $0.86\ \mu m$ and $2.13\ \mu m$ solar reflectances over a cirrus uncinus scene produced by the 3DCLOUD model. Then, 3D radiative transfer simulations are performed by the 3DMCPOL code at spatial resolutions ranging from 50 m to 10 km, for twelve viewing geometries and nine solar geometries. It is found that, for simulated nadir observations taken at resolution higher than 2.5 km, horizontal radiation transport (HRT) dominates biases between 3D and 1D reflectance calculations, but it is mitigated by the side illumination effect for off-zenith solar geometries. At resolutions coarser than 2.5 km, PPHB dominates. For off-nadir observations at resolutions higher than 2.5 km, the dominant effect is that the oblique line of sight passes through many cloud columns, but other 3D effects are also important. Similar to nadir simulations, side illumination effects mitigate the HRT. At resolutions coarser than 2.5 km, the PPHB is again the dominant effect. The magnitude and resolution-dependence of PPHB and IPAB is very different for visible, near-infrared, and shortwave infrared channels compared with the thermal infrared channels discussed in Part I

Atmos. Chem. Phys. Discuss., https://doi.org/10.5194/acp-2018-38
Manuscript under review for journal Atmos. Chem. Phys.
Discussion started: 6 February 2018


Atmospheric Chemistry and Physics Discussions

of this study. This strong wavelength dependency of cirrus cloud 3D radiative effects may be a significant issue for retrieval techniques that simultaneously use radiative measurements across a wide range of solar reflectance and infrared wavelengths.

## 1 Introduction

Clouds cover between 60 to 70 % of the Earth's surface and are one of the principal actors in the Earth's radiative budget (Intergovernmental Panel on Climate Change (IPCC) assessment report 5 Boucher et al. (2013)). On average, they lead to a net radiative effect of about $-20\ W.m^{-2}$ (Ramanathan et al., 1989) but this estimation depends on the global circulation model (GCM, Lane et al. (2000); Dufresne and Bony (2008)). It is therefore necessary to better understand clouds and their interaction with radiation. As part of the wide diversity of clouds, high altitude clouds such as cirrus play an important role in the climate and on the Earth's radiation budget (Hartmann and Short (1980); Ohring and Clapp (1980); Liou (1986); Stephens (2005); Eguchi et al. (2007)). They cover a large part of the Earth's surface (15 % to 40 %, Sassen et al. (2008)) and their high altitude implies a large difference between the cloud top and Earth's surface temperature. Such large difference produces an efficient greenhouse effect by trapping part of the infrared radiation emitted by the surface. Meanwhile, part of the solar incident radiation is reflected to space due to the albedo effect, particularly when the optical thicknesses is large (greater than 10, (Choi and Ho, 2006)). Most of the cirrus are optically thin (optical thickness less than 3 at 532 nm, Sassen et al. (2008)), leading to an average positive radiative effect (e.g. a greenhouse effect) of about $+28\ W.m^{-2}$ (Boucher et al., 2013). However, their radiative impact depends on numerous factors such as, cloud altitude (Corti and Peter, 2009), cloud thickness (Jensen et al., 1994), crystal shape and size parameter (Min et al., 2010) and temperature (Katagiri et al., 2013). Furthermore, in contrast to the light scattering by spherical water droplets which can be solved using the Mie theory, there is no exact solution for ice crystal scattering due to the multiplicity of crystal sizes and shapes (Lynch et al. (2002)).

Passive satellite sensors are well suited for global temporal and spatial observations of clouds, but the number of retrievable cloud parameters is limited, on the one hand, by the information content of the radiative measurements and, on the other hand, by the retrieval methods. Cloud optical thickness (COT) and cloud effective particle radius (CER) can be retrieved from space-based radiometric measurements using dedicated operational algorithms. Most algorithms are developed for solar-reflectance bands, like the operational algorithm of the Moderate Resolution Imaging Spectroradiometer (MODIS, Platnick et al. (2017)) for the MOD06 product; Minnis et al. (2011) for the CERES product). Currently, operational constraints such as time constraints or the lack of information regarding the 3 dimensional (3D) structure of clouds necessitate the use of a simplified cloud when operationally retrieving cloud properties. In one approach for processing the observations from an area, clouds are considered flat and homogeneous over the entire area. This hypothesis is named the homogeneous plane parallel approximation (PPHA, Cahalan et al. (1994)). If each cloudy pixel is considered flat, homogeneous and independent of its neighbors this is the homogeneous independent pixel approximation (IPA , Cahalan et al. (1994)) or homogeneous independent column approximation (ICA, Stephens et al. (1991)). Such representation implies that no interaction between pixels or cloudy columns is taken into account between the assumed homogeneous pixels. This is often far from the reality, where clouds have complex



three dimensional and heterogeneous structures and where the radiative transfer occurs in 3D, and can lead to errors in cloud property retrievals.

Therefore, a means for quantifying the impact of realistic cloud heterogeneities is necessary to begin to understand potential cirrus retrieval errors. Numerous studies have examined this issue for cloud products derived from solar spectral reflectance measurements, but mainly for warm liquid water clouds (e.g. stratocumulus clouds). Indeed, Varnai and Marshak (2001); Zinner and Mayer (2006); Kato and Marshak (2009) and Zhang and Platnick (2011) (and references therein) have shown that neglected cloud horizontal and vertical inhomogeneities can lead to an erroneous albedo or top of the atmosphere (TOA) reflectances depending on numerous factors such as sensor spatial resolution, the wavelength range, observation geometry, and cloud type, etc. Concerning cirrus clouds in the solar spectral range, Buschmann et al. (2002) found that, for cirrus clouds with mean optical thicknesses smaller than 5 and with relative optical thickness variances smaller than 0.2, retrieval errors due to the cloud homogeneous assumption are smaller than $\pm 10\%$. Carlin et al. (2002) showed that, due to horizontal cirrus inhomogeneity, both solar albedo and outgoing long wave radiation biases could reach 15 $W.m^{-2}$ in magnitude. Using spectral irradiance measurements below and above tropical cirrus, Schmidt et al. (2009) showed that solar radiation in the visible is significantly decreased due to net horizontal radiation transport, especially near cloud edges. Zhang et al. (2010) showed that the vertically homogeneous column assumption used in solar reflectance bi-spectral and thermal infrared retrieval techniques may lead to underestimates of COT and CER of thin cirrus due to the non-linear dependance of ice crystal scattering properties on the effective size. More recently, Fauchez et al. (2012, 2014) showed that 3D thermal infrared (TIR) brightness temperatures (BT) at TOA can be up to 15 K greater than those computed from a 1D radiative transfer code. Fauchez et al. (2015) showed that cirrus heterogeneity effects can significantly influence cirrus optical property retrievals (up to $20\%$ for COT and $100\%$ for CER retrievals) at the 1 km scale of MODIS TIR observations. In the TIR, BT and retrieval differences due to cloud inhomogeneities and 3D effects are mainly dependent on the standard deviation of optical thickness within a 1 km pixel. Thus, at the 1 km scale, the differences between 3D radiative transfer from heterogeneous pixels and 1D radiative transfer from homogeneous pixels are mainly dominated by the failure of the PPHB .

Most of these previous studies have been performed at the typical 1 km nadir spatial resolution of polar orbiting imagers. However, the impact of the cloud homogeneous assumption depends on the scale at which the cloud is considered homogeneous. For liquid water clouds Davis et al. (1997) have examined cloud heterogeneities as a function of scale for stratocumulus clouds. They highlighted that the impact of the cloud inhomogeneities on the optical thickness retrieval is at a minimum around 1 or 2 km resolution. Indeed, on the one hand, the 3D radiative impact increases at finer spatial resolutions because the photon mean path becomes as large or larger than the pixel size. On the other hand, at coarser spatial resolutions, the plane parallel and homogeneous bias (PPHB) is enhanced because the pixel becomes larger than the homogeneity scale. In addition, Zhang et al. (2012) showed that at 100 m spatial resolution, 3-D radiative transfer effects on CER retrieval, such as side illumination and shadowing, are much larger at 2.1 than 3.7 $\mu m$ but because side illumination and shadowing effects almost cancel out each other, there is an overall agreement between CER retrieved using 2.1 or 3.7 $\mu m$. However, at resolutions similar to MODIS,

Atmos. Chem. Phys. Discuss., https://doi.org/10.5194/acp-2018-38
Manuscript under review for journal Atmos. Chem. Phys.
Discussion started: 6 February 2018


Atmospheric Chemistry and Physics Discussions

while both 3D effects cancel each other out, CER retrieved at 2.1 $\mu m$ is systematically larger than at 3.7 $\mu m$ when averaged over the LES domain because of cloud horizontal inhomogeneity (PPHB). These results are important for assessing the overall retrieval errors from various space-borne imagers having different spatial resolutions and determining, if possible, which resolution is better to mitigate the effects of cloud heterogeneities on radiance measurements.

In Part I of our study, Fauchez et al. (2017a) discussed the impact of ice cloud (cirrus) heterogeneities as a function of pixel size by simulating MODIS thermal infrared channel measurements. It was shown that the spatial resolution range where the combination of heterogeneity and 3D effects is minimum falls between 100 m and 250 m. In Part II of this study, we focus our attention on simulating MODIS visible-near-infrared (VNIR) and shortwave infrared (SWIR) reflectance measurements in the 0.86 $\mu m$ and 2.13 $\mu m$ MODIS channels, respectively; these channels are currently used to retrieve cloud optical properties over water surfaces in MOD06 (Platnick et al., 2017). Effects of cloud heterogeneity are studied for different viewing and solar angles as a function of spatial resolutions ranging from 50 m to 10 km.

In Section 2, we briefly describe the cloud generator model 3DCLOUD (Szczap et al. (2014)) and the 3D radiative transfer model 3DMCPOL (Cornet et al. (2010), Fauchez et al. (2012, 2014)) used to simulate the 3D radiative transfer for heterogeneous cirrus clouds. In Section 3 we describe the cloud heterogeneity effects for solar reflectance channels. In Section 4 we study the dependence of horizontal heterogeneity effects on spatial resolution and observation geometry. Summary and conclusions are given in Section 5.

## 2 Simulation of 3D radiative transfer through a realistic 3D heterogeneous cirrus field

The single cirrus field modeled in this paper is identical to the one presented by Fauchez et al. (2017a) in Part I. This allows comparisons of those TIR results presented in Part I (Fauchez et al., 2017a) with the VNIR/SWR results in this Part II. The cirrus is modeled with the 3DCLOUD (Szczap et al. (2014); Alkasem et al. (2017)) model that simulates 3D cloud structures by assimilating meteorological profiles and by solving simplified basic atmospheric equations. The scale invariant properties observed for clouds are then constrained to follow a -5/3 spectral slope (Hogan and Kew (2005), Szczap et al. (2014)) using a Fourier filtering method. This method ensures that the horizontal variation of the ice water content (IWC) is consistent with observations (Hogan and Kew (2005); Fauchez et al. (2014)).

The radiative transfer simulations are then performed using the 3DMCPOL Monte Carlo radiative transfer (RT) code (Cornet et al. (2010), Fauchez et al. (2012, 2014)). Cirrus optical properties are parametrized using the same microphysical model assumed by the MODIS Collection 6 (MOD06) cloud product, namely the severely roughened single-habit column aggregate from Yang et al. (2013). The domain mean optical thickness of the 3DCLOUD cirrus is 1.5 at 0.86 $\mu m$, and the cloud is assumed to have a constant CER of 10 $\mu m$. The optical properties of the assumed ice crystal used at two MODIS channels are

Atmos. Chem. Phys. Discuss., https://doi.org/10.5194/acp-2018-38
Manuscript under review for journal Atmos. Chem. Phys.
Discussion started: 6 February 2018




shown Table 1.

Solar reflectances are computed with 3DMCPOL for MODIS channel 2 (centered at $0.86\ \mu m$) and 7 (centered at $2.13\ \mu m$). Five solar geometries are considered: ($\Theta_s = 0°$; $\Phi_s = 0°$), ($\Theta_s = 30°$; $\Phi_s = 0°$, $90°$ and $180°$) and ($\Theta_s = 60°$; $\Phi_s = 0°$) with $\Theta_s$ and $\Phi_s$ corresponding to solar zenith and azimuth angles, respectively. For each of these angles twelve viewing geometries are computed: three view zenith angles: $\Theta_v = 0°$, $30°$ and $60°$ with four view azimuth angles each: $\Phi_v = 0°$, $45°$, $90°$ and $180°$. The azimuths of viewing angles relative to the cirrus field are represented in Figure 1. This figure shows the cirrus cloud field simulated by 3DCLOUD based on the mid latitude summer meteorological profiles already used in Fauchez et al. (2017a). Top panels show the vertical profiles of ice water content (IWC) along the red lines in the optical thickness field shown in the bottom panels for different viewing angles. Note that the cirrus vertical profile looks very different as a function of the viewing geometry. The wind direction is following the $\Phi_v = 45°$ arrow leading to clearly visible virga features at this angle. Note that the azimuth view angles $\Phi_v = 225°$ and $270°$ are shown on this figure for comparison to others angles, but are not computed for computational time reasons.

Figure 2 (a) shows the cirrus optical thickness field at $0.86\ \mu m$ at 50 m spatial resolution, and (b) shows the corresponding 3D reflectance field at nadir in (b). 100 billion of fictive light particles (FLIPs (Pujol, 2015), referenced hereafter as photons) are computed in 13 hours on the NCCS discover supercomputer (see acknowledgements) for 3D computations of the solar reflectance within an accuracy of about $0.1\%$.

## 3 Decomposition of the effects of cloud heterogeneity and 3D radiative transfer on simulated reflectances

Clouds are complex 3D structures where solar and terrestrial radiation follow 3D paths. However, in current retrieval algorithms, for simplification and/or computational reasons, the independent pixel approximation (IPA, Cahalan et al. (1994)) is commonly applied: each portion of the observed cloudy scene is sampled in pixels, and each pixel is assumed to be horizontally and vertically homogeneous as well as radiatively independent of its neighbors (1D radiative transfer assumption). To study cirrus heterogeneities that can affect solar reflectances, we simulate 1D solar reflectances with 3DMCPOL following the common homogeneous IPA retrieval assumption. COT is first averaged from the highest spatial resolution (50 m) to the spatial resolution of interest (up to 10 km) before performing the 1D RT calculations. Conversely, 3D reflectances are always computed at 50 m and are then aggregated to a given spatial resolution (from 50 m to 10 km). The difference $\Delta R$ between 3D and 1D reflectances obtained this way corresponds to the combined impact of cloud heterogeneities and 3D RT on the TOA reflectances.

However, it is useful to distinguish the following different effects and radiative processes that impact cloud-top reflectances when 3D RT inside heterogeneous pixels are compared to 1D RT inside homogeneous pixels:

Atmos. Chem. Phys. Discuss., https://doi.org/10.5194/acp-2018-38
Manuscript under review for journal Atmos. Chem. Phys.
Discussion started: 6 February 2018


Atmospheric Chemistry and Physics Discussions

1. The Plane-Parallel and Homogeneous Bias assumption (PPHB)
2. Optical property vertical inhomogeneity (not considered here)
3. The Tilted and Homogeneous Extinction Approximation Bias (THEAB)
4. 3D radiative effects due to the non-radiative independence of the pixels

**Plane-parallel and homogeneous assumption bias (PPHB):** In current operational satellite retrieval algorithms, the scene within each observed pixel is assumed to be horizontally homogeneous. The impact of the horizontal heterogeneity clearly depends on the sensor spatial resolution (Oreopoulos and Davis, 1998). In Fig. 3 we plot the reflectances $R_{50m}^{1D}$ estimated with a 1D RT calculation at 50 m for $0.86\ \mu m$ and $2.13\ \mu m$ channels, respectively, as a function of the 50 m $0.83\ \mu m$ optical thickness ($\tau_{50m}^{0.8}$) at 50 m. We see that the relation between reflectance and optical thickness is increasing (the thicker is the cloud, the more light is reflected) but non-linear. Indeed, between two reflectances $R1D_1$ and $R1D_2$, the averaged reflectance, $\overline{R1D}$ corresponds to a smaller optical thickness $\tau$ than the averaged optical thickness corresponding to the two reflectances. This is the Jensen's inequality (Newman et al., 1995), usually called the plane-parallel and homogeneous bias (PPHB, Cahalan et al. (1994); Cahalan et al. (1995), Oreopoulos and Davis (1998)). Note that we plot 1D reflectances and not 3D ones only to highlight the effect of the PPHB.

**Vertical inhomogeneity (not considered here):** For the same optical thickness, the vertical distribution of the ice crystal CER and IWC may have an impact on TOA reflectances and retrieved CER. For instance, Zhang et al. (2010) showed that the vertically homogeneous column assumption used in solar reflectance bi-spectral and thermal infrared retrieval techniques may lead to underestimates of COT and CER of thin cirrus due to the non-linear dependance of ice crystal scattering properties on the effective size. However, because in this study we are interested in the impact of the space sensor horizontal spatial resolution on TOA VNIR/SWIR reflectances, we do not consider the vertical heterogeneity.

**Tilted and homogeneous extinction approximation bias (THEAB):** This effect concerns off-nadir geometries. At the spatial resolution of a spaceborne imager, the tilted line of sight can cross several atmospheric columns above the surface for a single observed cirrus pixels, while in the operational algorithms, each cloudy column is assumed horizontally infinite and homogeneous. This effect can lead to a smoothing of the radiative field because each line of sight encounters many cloudy columns (of various optical properties), and overall the total optical path along each line of sight is equivalent leading, on average, to a more homogeneous view. See for example Várnai and Davies (1999); Varnai and Marshak (2003), Kato and Marshak (2009).

**3D radiative effects:** In addition to the impact of the heterogeneity in the cloudy column, the IPA can lead to significant retrieval errors due to the horizontal photon transport between nearby columns (Várnai and Davies (1999); Varnai and Marshak (2001, 2003); Marshak and Davis (2005), Oreopoulos and Cahalan (2005), Kato and Marshak (2009), etc.). Indeed, for

Atmos. Chem. Phys. Discuss., https://doi.org/10.5194/acp-2018-38
Manuscript under review for journal Atmos. Chem. Phys.
Discussion started: 6 February 2018


Atmospheric Chemistry and Physics Discussions

3D radiative transfer, photons can cross several cloudy columns having different optical properties (though horizontal transport depends strongly on particle absorption and so can vary widely between VNIR and SWIR imager channels for the same pixel, e.g., (Platnick, 2001). Several distinct categories of 3D effects are worth mentioning:

1. **Horizontal radiation transport (HRT)** (Davies (1978), Kobayashi (1993),Davis and Marshak (2001), Várnai and Davies (1999); Varnai and Marshak (2003)): photons can be transported from one cloud column to another. Marshak et al. (1995) have determined that the radiative smoothing scale $L$ due to photon horizontal transport (or photon diffusion) is expressed by $L = H \times \sqrt{(1-g)COT}$ where $H$ is the cloud geometrical thickness, COT the optical thickness and "g" the asymmetry parameter of the phase function. It has been found that the escapes of photons of the cloud (leakage effect) are concentrated where the optical thickness is the thinnest because, first, photons in thin columns have less chance to be absorbed or scattered toward another column and, second, because photons in neighboring columns with stronger scattering have more chance to leave the cloud if they are scattered toward a neighboring column with a smaller extinction coefficient. This increases the reflectance of optically thin pixels and decreases the reflectance of optically thick ones. Figure 4 (a) shows nadir reflectances at 50 m ($R_{50m}$) as a function the optical thickness $\tau^{0.86\ \mu m}$ in 3D and 1D for channels centered at $0.86\ \mu m$ and $2.13\ \mu m$ for solar zenith angles of $\Theta_s = 0°$. For zenith sun we can see that for small $\tau^{0.86\ \mu m}$ ($\leq 2$) 3D reflectances are larger than 1D reflectances while for larger $\tau^{0.86\ \mu m}$, 3D reflectances are smaller than 1D reflectances due to the HRT.

2. **Side illumination effect** (Wendling (1977), Cahalan et al. (1994), Varnai and Marshak (2003), Zhang et al. (2012)): This effects occurs when photons of the incoming sunlight travel obliquely which globally increases the reflectance of the cloud by comparison to what is expected in the 1D theory (Loeb and Davies, 1996) as we can see Fig.4 (c) for which most of the 3D reflectances are larger than 1D reflectances. This effect is stronger for the large optical thicknesses and tends also to block photons in the thickess regions before they reach the thinnest neighbor regions. Note that 3D reflectances are closer to 1D reflectances values for $\Theta_v = 60°$ than for an overhead sun (Fig. 4a) for this range of optical thickness.

3. **Shadowing effect** (L. H. Chambers (1997), Zuidema and Evans (1998), Varnai and Marshak (2003), Zhang et al. (2012)): As for side illumination, this effect occurs when sunlight photons traveled slantwise, but this time, photons first reach a cloudy column with a large extinction, depriving neighbor cloudy columns from incoming photons.

The first 3D effect acts to smooth the radiation field structure, whereas the second and the third effects lead to a roughening effect of the radiation field. Smoothing is an isotropic effect accounting for large scattering orders, whereas roughening acts mainly in the solar plane by direct and low order scattered sunlight (Zuidema and Evans (1998); Varnai and Marshak (2003); Oreopoulos and Cahalan (2005)). Also, the side illumination effect is usually larger than the shadowing effect (Varnai and

Atmos. Chem. Phys. Discuss., https://doi.org/10.5194/acp-2018-38
Manuscript under review for journal Atmos. Chem. Phys.
Discussion started: 6 February 2018


Atmospheric Chemistry and Physics Discussions

Marshak (2003)). On average, large optical thickness are more highlighted from the side but they also block part of the photons from reaching the neighboring columns.

Note that all of these effects are dependent on the cloud optical thickness heterogeneity, the vertical inhomogeneity of the volume extinction, the variation of the cloud top and base altitude (always considered flat in our study) as well as the solar and viewing angles. All combined together, the total effect due to cloud inhomogeneity and 3D radiative transfer are very complex and dependent on the spatial resolution.

## 4 Cirrus horizontal inhomogeneity and 3D effects as a function of the observation scale

### 4.1 Plane parallel and homogeneous bias

When all the various effects relative to pixel optical property inhomogeneity, radiation transport, and oblique viewing geometries act together, it is difficult to separate their relative contributions. Following Varnai and Marshak (2003), the horizontal inhomogeneity effects due to the PPHB can be isolated from 3D effects by using 1D radiative transfer calculations. Nadir 1D reflectances aggregated from the native spatial resolution (50 m) can be compared to reflectances computed at a given spatial resolution following the homogeneous pixel assumption. This is expressed by Eq. 1 and is shown in Fig. 5.

$$\overline{\Delta R}(\overline{1D_{50m\ R}} - 1D_{\bar{\tau}}) = [\sum_{i=1}^{N}(\overline{R^{1D}_{50m\ R}}^{xkm} - R^{1D\ xkm}_{\bar{\tau}})]/N, \quad (1)$$

where $\overline{1D_{50m\ R}}$ denotes the averaged 1D radiances computed at 50 m and $1D_{\bar{\tau}}$ the 1D radiances computed at the $xkm$ averaged optical thickness $\bar{\tau}$.

The finest spatial resolution for this figure is at 100 m because at 50 m (native spatial resolution) there are no aggregated reflectances. As we can expect, the PPHB increases as the spatial resolution increases with the largest $\overline{\Delta R}(\overline{1D_{50m}} - 1D_{\bar{\tau}})$ at 10 km spatial resolution, i.e. when the entire cloud field is assumed homogeneous. As we have already seen in Fig. 3, in most of the optical thickness range ($\geq 2$), the PPHB leads to aggregated reflectances smaller than the reflectances computed for the averaged optical thickness, such that, on average, $\overline{\Delta R}(\overline{1D_{50m}} - 1D_{\bar{\tau}}) < 0$. Also, we can see that the PPHB increases with increasing solar zenith angle (moving from (a) to (c)). Indeed, the non-linearity of the reflectance vs. COT relation increases with the solar zenith angle (compare the blue or green curves of 1D reflectances in Fig. 4 (a) and (c)) making the PPHB (which arise from this nonlinearity) much stronger. Note that for sun at zenith, the PPHB effect is tiny, almost 0 except for large viewing zenith angles ($\Theta_v = 60°$, blue lines) where the extinction is very large along the line of sight. This conclusion is different from Varnai and Marshak (2003) because cirrus optical thickness is, on average, smaller than stratocumulus optical thicknesses leading to a weaker PPHB, which is overall very weak for nadir views at all spatial resolutions. In addition, this conclusion is also drastically different from that of Fauchez et al. (2017a) for thermal infrared wavelengths, where the PPHB dominates beyond about 250 m. Indeed in the TIR, the cloud absorption is larger and the source of radiative emission is not the Sun but

Atmos. Chem. Phys. Discuss., https://doi.org/10.5194/acp-2018-38
Manuscript under review for journal Atmos. Chem. Phys.
Discussion started: 6 February 2018




the atmosphere, cloud and surface. Furthermore, the large temperature difference between the cirrus and the surface leads to large brightness temperatures inhomogeneities and therefore large PPHB.

### 4.2 Tilted and homogeneous extinction approximation bias (THEAB)

When the view zenith angle is large, the THEAB may also significantly impact the difference between TOA reflectances estimated with the 1D horizontal homogeneous cloud assumption and those corresponding to the reality of the 3D radiative transfer. For cloud observations from TOA, an oblique line of sight may cross many different cloudy columns, while the 1D plane parallel and homogeneous assumption considers only a single cloudy column above the observation pixel, assumed horizontally infinite. The THEAB is therefore a consequence of the PPHB for oblique view. To highlight only the THEAB without considering the horizontal radiative transport effect we compared 1D reflectances computed with the homogeneous, independent and infinite pixel assumption (named $1D_{\bar{\tau}}$) to those computed with the independent but non-infinite pixel assumption (named $1D_{o.e\bar{\tau}}$ for oblique extinction). In the latter situation the line of sight is allowed to cross neighboring cloudy columns, but the columns are still radiatively independent (i.e. this is not 3D RT). For each pixel we have re-created a 1D cloud for which the vertical extinction is the averaged oblique extinction of the 3D heterogeneous field. In other words, we have run 1D RT using the oblique columns crossed as adjacent vertical cloud layers (i.e., tilted the oblique columns crossed to a vertical column). It is important to mention here that when the line of sight is very slant, the variety of voxel extinctions from a line of sight to another can be quite similar. Overall, each of them cross large, medium and small extinctions leading to similar optical path and therefore a more homogeneous field of view than for the 1D plane-parallel assumption where only a unique homogeneous column is crossed. The relative and absolute differences are estimated following equations 2 and 3, respectively, are represented in Fig. 6 (a), and (b), respectively.

$$\overline{\Delta R}(1D_{o.e.\ \bar{\tau}} - 1D_{\bar{\tau}}) = [\sum_{i=1}^{N}(R_{\bar{\tau}}^{1Dxkm\ o.e.} - R_{\bar{\tau}}^{1Dxkm})]/N, \tag{2}$$

$$\overline{|\Delta R|}(1D_{o.e.\ \bar{\tau}} - 1D_{\bar{\tau}}) = [\sum_{i=1}^{N}(|R_{\bar{\tau}}^{1Dxkm\ o.e.} - R_{\bar{\tau}}^{1Dxkm}|)]/N, \tag{3}$$

In Fig. 6 we see, as expected, that for oblique sun and off-nadir view the THEAB is the largest for the finest spatial resolutions, because the pixel size is small and thus an oblique line of sight can cross many different columns during its paths through the cloud. There is a small dependence on the view azimuth angle with the largest effect at $\phi_v = 180°$. The THEAB is more important for large view zenith angles because the number of columns crossed by the line of sight increases with the view zenith angle. THEAB also increases with the solar zenith angle from $30°$ to $60°$ for much the same reasons. At a pixel size of 2.5 km, the large pixel size reduce the THEAB, which becomes almost null, since less different cloudy columns are crossed. The PPHB thus becomes the dominant effect. Note that the spatial resolution from which the THEAB becomes almost null

Atmos. Chem. Phys. Discuss., https://doi.org/10.5194/acp-2018-38
Manuscript under review for journal Atmos. Chem. Phys.
Discussion started: 6 February 2018


Atmospheric Chemistry and Physics Discussions

will depend on the horizontal extension and geometrical thickness of the cloud. The horizontally longer and/or geometrically thicker the cloud is the coarser will be the spatial resolution at which the THEAB becomes insignificant.

### 4.3 Horizontal heterogeneity and 3D effects

In nature, radiative transfer occurs in 3D not in 1D. Therefore, in addition to the PPHB, 3D radiative effects influence the spectral reflectance of a given pixel due to its radiative connection between neighbors. 3D effects include various effects such as the HRT between cloudy columns or side illumination and shadowing effect for oblique Sun illumination. To compare reflectances issue from a 3D radiative transfer through a heterogeneous pixel with reflectances from the 1D homogeneous pixel assumption, we estimate the arithmetic mean difference between aggregated 3D and non-aggregated (coarser-resolution) 1D reflectances as follows:

$$\overline{\Delta R}(\overline{3D_{50m\ R}} - 1D_{\bar{\tau}}) = [\sum_{i=1}^{N}(\overline{R^{3D}_{50m\ R}}^{xkm} - R^{1D\ xkm}_{\bar{\tau}})]/N, \tag{4}$$

with $\overline{3D_{50m\ R}}$ the averaged 3D radiances computed at 50 m, $1D_{\bar{\tau}}$ the 1D radiances computed at the $xkm$ averaged optical thickness $\bar{\tau}$ and $N$ the number of pixels at the spatial resolution $xkm$. Note that because the PPHB is already included in Eqs. 1, the comparison here shows how the nonlinearity between reflectance and optical thickness, combined with 3D radiative effects and solar geometries, affects TOA reflectances for a given view angle and spatial resolution.

Some effects such as the HRT may, on average, have an almost nil effect but locally, at the pixel scale, have large positive and negative magnitudes. We therefore estimate the absolute magnitude of the total effect by calculating the absolute mean difference between aggregated 3D and non-aggregated 1D reflectances as follows:

$$\overline{|\Delta R|}(\overline{3D_{50m\ R}} - 1D_{\bar{\tau}}) = [\sum_{i=1}^{N}(|\overline{R^{3D}_{50m\ R}}^{xkm} - R^{1D\ xkm}_{\bar{\tau}}|)]/N, \tag{5}$$

Figure 7 shows $\overline{\Delta R}(\overline{3D_{50m}} - 1D)$ (panels (a), (b) and (c)) and $\overline{|\Delta R|}(\overline{3D_{50m}} - 1D)$ (panels (d), (e) and (f)) at $0.86\ \mu m$ as a function of the solar zenith angle $\Theta_s$ for spatial resolutions from 50 m to 10 km and for various viewing angles. First of all, we see that, $\overline{\Delta R}(\overline{3D_{50m}} - 1D)$ is on average negative, mainly due to the HRT (see Fig. 4) and PPHB for optical thicknesses larger than 5 (see Fig. 3). However, at $\Theta_v = 60°$ we can see that $\overline{\Delta R}(\overline{3D_{50m}} - 1D)$ changes sign. This is because of the THEAB which is a positive bias, stronger at high resolutions and large view angles (see Fig 6). Indeed, as previously stated, in 3D RT the HRT acts mostly by moving photons from thick to thin areas leading to an increase of reflectances for small optical thicknesses and a decrease of reflectances for large optical thicknesses in comparison to 1D RT. Furthermore, $\overline{|\Delta R|}(\overline{3D_{50m}} - 1D)$ is, on average, decreasing with $\Theta_s$ (except at $\Theta_v = 60°$; $\Phi_v = 180°$) because the PPHB is stronger (at coarser resolutions, cf. Fig 5 (d), (e) and (f)) and because the HRT from thick to thin areas is mitigated by the side illumination effect (at higher spatial resolutions). Indeed, in 3D, the side illumination effect leads to many photons being first intercepted by thick regions, without

Atmos. Chem. Phys. Discuss., https://doi.org/10.5194/acp-2018-38
Manuscript under review for journal Atmos. Chem. Phys.
Discussion started: 6 February 2018


Atmospheric Chemistry and Physics Discussions

reaching thin regions, contrary to cases with an overhead Sun. This leads to a larger reflectance in thick regions and to a smaller reflectance in thin regions, but on average, 3D reflectances at $\Theta_v = 60°$ are closer to 1D reflectances than for an overhead Sun (see Fig. 8 for illustration).

For nadir view, $\overline{\Delta R}(\overline{3D_{50m}} - 1D)$ and especially $\overline{|\Delta R|}(\overline{3D_{50m}} - 1D)$ tend to be the smallest (because of no THEAB), and almost constant over the spatial resolutions and $\Theta_s$.

For oblique views, the larger the viewing zenith view angle $\Theta_v$, the larger is $\overline{|\Delta R|}(\overline{3D_{50m}} - 1D)$ (see THEAB in section 4.2), except for $\Phi_v = 45°$. This view is directly parallel to the fallstreaks of the cirrus, where the variability along the line of sight is the smallest (see Fig. 1 (b) and (e)). We can also see that due to the THEAB, $\overline{\Delta R}(\overline{3D_{50m}} - 1D)$ is positive for $\Theta_v = 60°$ for several $\Phi_v$ for the highest spatial resolutions. Indeed by comparing these results with those of Fig. 6, we can see that, for spatial resolutions below 1 km, the THEAB is the dominant effect for large solar zenith angles. The absolute THEAB effect $\overline{|\Delta R|}(1Do.e - 1D)$ is even larger than the total effect $\overline{|\Delta R|}(\overline{3D_{50m}} - 1D)$ which is reduced by the radiative smoothing.

Figure 9 shows $\overline{\Delta R}(\overline{3D_{50m}} - 1D)$ (panels (a), (b) and (c)) and $\overline{|\Delta R|}(\overline{3D_{50m}} - 1D)$ (panels (d), (e) and (f)) at 2.13 $\mu m$ as a function of the solar zenith angle $\Theta_s$ for spatial resolutions from 50 m to 10 km and for various viewing angles. Comparing with Fig. 7 for 0.86 $\mu m$ reflectances we can see that the amplitude of $\overline{\Delta R}(\overline{3D_{50m}} - 1D)$ and $\overline{|\Delta R|}(\overline{3D_{50m}} - 1D)$ are smaller at 2.13 $\mu m$ for low solar zenith angles ($\Theta_s = 0$ and 30°). Indeed because of the larger cloud absorption in the SWIR channel, the HRT is reduced. But at $\Theta_s = 60°$ the cloud extinction is also strong at 0.86 $\mu m$, leading to similar $\overline{\Delta R}(\overline{3D_{50m}} - 1D)$ and $\overline{|\Delta R|}(\overline{3D_{50m}} - 1D)$ amplitudes. Because the effects are similar between the VNIR and SWIR channels, in the later figures we only focus on the VNIR channel centered 0.86 $\mu m$ to avoid overloading the manuscript.

In Fig. 10, we can see the influence of the solar azimuth angle on $\overline{\Delta R}$ and $\overline{|\Delta R|}$. For this particular cloud geometry, the largest $\overline{\Delta R}$ and $\overline{|\Delta R|}$ is for a solar azimuth angle $\Phi_s = 180°$ because the side illumination effect is the strongest in forward scattering. However, the differences are relatively small over the solar azimuth angles because each of the three angles highlights the cirrus fallstreaks obliquely (see Fig. 1 to compare with viewing angles). Indeed, while cirrus clouds with fallstreaks are particularly heterogeneous as highlighted from different solar azimuth angles, the relative small optical thickness of cirrus does not lead to large azimuthal dependency.

Like other effects, the importance of 3D effects is dependent on the spatial resolution. It is complicated to represent their relative effect since they can either increase or decrease the reflectances (smoothing by HRT or roughening by side illumination and shadowing). However the mean deviation due to 3D effects at each spatial resolution can be obtained by subtracting the absolute value of PPHB ($\overline{|\Delta R|}(\overline{1D_{50m}} - 1D)$, the THEAB being already include in the PPHB) from the total absolute mean difference $\overline{|\Delta R|}(\overline{3D_{50m}} - 1D)$ such as 3D effects= $\overline{|\Delta R|}(\overline{3D_{50m}} - 1D)$ - PPHB.

Figure 11 represents the absolute values |3D effects| as a function of the spatial resolution for solar angles $\Theta_s$ from 0 to 60° with the solar azimuth angle set at $\Phi_s = 0°$ and for a various view angles. In contrast to the PPHB, 3D effects are large for small pixel sizes and then decrease with coarsening spatial resolutions. Indeed, at small pixel sizes, photons with a given mean



free path can cross a lot of pixels. Comparing with the absolute THEAB in Fig. 6, the absolute 3D effects are slightly smaller and follow the same decreasing with coarsening spatial resolutions. Note that the dependence on the view azimuth angle is due to the fall streak structure of this particular cirrus field.

## 5 Conclusions

In this work we have modeled a cirrus cloud with the 3DCLOUD model with typical characteristics. Only one cirrus structure has been modeled for computation time reasons, but many spatial resolutions, view and solar angles have been considered. However, the radiative process discussed here can be extrapolated to other cirrus clouds, with some differences depending on cirrus structure (fallstreaks or not), solar and view geometries, averaged optical thickness etc. Simulation of the radiative transfer through this scene have been performed with the 3DMCPOL code for 0.86 and $2.13\mu m$ reflectances for various configurations: 1) Full 3D radiative transfer at high spatial resolution, 2) 1D radiative transfer at various spatial resolutions for which the extinction variability along the oblique line of sight is take into account (like in 3D), 3) Vertically homogeneous 1D radiative transfer at various spatial resolutions. The spatial resolutions considered here are ranged from 50 m to 10 km. By comparing the results of these simulations, the paper examined three types of effects: the plane-parallel and homogeneous approximation bias (PPHB) due to the non-linear relationship between optical thickness and reflectance, the 3D effects due to the transport of photons between pixels as well as side illumination and shadowing effects for oblique Sun, and the tilted and homogeneous extinction approximation bias (THEAB) due to the fact that in 1D the line of sight is assumed to remain in a single vertical column, while in reality, it can cross many different cloudy columns. The relative contribution of these three effects on the TOA reflectances is strongly dependent on spatial resolution but also on cloud structure. No particular differences have been noticed between 0.86 and 2.13 $\mu m$ channels (except magnitude of the effect), therefore, for clarity, most of the figures shown the $0.86$ $\mu m$ channel only. For the particular configuration of a cirrus uncinus we have shown the following points:

- For nadir observations:
  - Below 2.5 km spatial resolution, 3D effects are dominant.
    - For overhead Sun, HRT is the only 3D effect.
    - For oblique Sun, side illumination effect mitigates the HRT from thick to thin regions leading to smaller differences between 3D and 1D reflectances.
  - At spatial resolution coarser than 2.5 km, the PPHB is the dominant effect.
- For an observation off-nadir:
  - Similar conclusion to nadir observations except that below 2.5 km spatial resolution, the dominant effect is THEAB, rather than 3D effects.



For off-nadir observations, the THEAB is very large for high spatial resolutions (small pixels, roughly bellow about 250 m), especially for a line of sight crossing the fallstreaks of cirrus uncinus. This bias is difficult to evaluate from observations, as this would need an active sensor, such as a lidar, looking at an oblique view angle. For low spatial resolutions (large pixel sizes, roughly > 2.5 km) the PPHB is the largest effect when compared to higher spatial resolutions. Note that this spatial resolution is different from that estimated by Davis et al. (1994) for stratocumulus clouds of roughly > 1 km due to the larger optical thickness of those clouds. Between this two ranges, competition between 3D effects, THEAB and PPHB is complicated and will depend on the cloud structure and the viewing and solar geometries. It is therefore difficult to generalize the conclusions for this intermediate range to other cirrus clouds. It is also important to notice the competition between the HRT from thick to thin regions, occurring regardless of the solar geometry versus side illumination effect which mostly increases the reflectance of large optical thicknesses, but blocks the photons from eventually reaching thinner neighbor regions. Overall the differences between 3D and 1D reflectances are mitigated when the solar zenith angles increases which is different from the conclusions of Loeb and Davies (1996) on thicker stratocumulus clouds. The overall predominant effect will therefore depend on the cloud optical thickness and viewing/solar geometries.

In Part I of this study, which focused on the impact of cloud inhomogeneity and 3D effects in thermal infrared channels, the PPHB has been found larger than 3D effects at resolutions coarser than 100-250 m. This is because the cloud absorption is much larger in the thermal infrared (TIR), leading to a larger PPHB even at relatively small pixel sizes. The differences between horizontal inhomogeneity and 3D effects at TIR and VNIR/SWIR channels pose a problem for retrieval techniques such as the optimal estimation method (OEM, Rodgers (2000)) that use multiple channels from these wavelength ranges (Fauchez et al., 2017b). In a future study, the impact of such differences in the retrieval of cirrus optical properties will be investigated using an OEM at five channels across the VNIR/SWIR/TIR ranges and at spatial resolutions ranging 50 m to 10 km.

*Code availability.* The simulated data used in this study were generated by the 3DCLOUD (Szczap et al. (2014)) and 3DMCPOL (Cornet et al. (2010); Fauchez et al. (2014)) closed-source codes. Please contact the authors for more information.

*Acknowledgements.* The authors acknowledge the Universities Space Research Association (USRA) through the NASA Postdoctoral Program (NPP) for their financial support.

We thank the UMBC High Performance Computing Facility (HPCF) for the use of their computational resources (MAYA). The facility is supported by the U.S. National Science Foundation through the MRI program (grant nos. CNS-0821258 and CNS-1228778) and the SCREMS program (grant no. DMS-0821311), with additional substantial support from the University of Maryland, Baltimore County (UMBC). See www.umbc.edu/hpcf for more information on HPCF and the projects using its resources.

We also thanks the NASA Center for Climate Simulation (NCCS) for the use of their computational resources (Discover).

Atmos. Chem. Phys. Discuss., https://doi.org/10.5194/acp-2018-38
Manuscript under review for journal Atmos. Chem. Phys.
Discussion started: 6 February 2018


Atmospheric Chemistry and Physics Discussions

## References

Alkasem, A., Szczap, F., Cornet, C., Shcherbakov, V., Gour, Y., Jourdan, O., Labonnote, L., and Mioche, G. Effects of cirrus heterogeneity on lidar CALIOP/CALIPSO data. *Journal of Quantitative Spectroscopy and Radiative Transfer*, **202**:38 – 49, 2017.

Benassi, A., Szczap, F., Davis, A., Masbou, M., Cornet, C., and Bleuyard, P. Thermal radiative fluxes through inhomogeneous cloud fields: a sensitivity study using a new stochastic cloud generator. *Atmospheric Research*, **72**:291–315, 2004.

Boucher, O., Randall, D., Artaxo, P., Bretherton, C., Feingold, G., Forster, P., Kerminen, V.-M., Kondo, Y., Liao, H., Lohmann, U., Rasch, P., Satheesh, S., Sherwood, S., Stevens, B., and Zhang, X. *Climate Change 2013: The Physical Science Basis. Contribution of Working Group I to the Fifth Assessment Report of the Intergovernmental Panel on Climate Change*, book section 7, pages 571–658. Cambridge University Press, Cambridge, United Kingdom and New York, NY, USA, 2013.

Buschmann, N., McFarquhar, G. M., and Heymsfield, A. J. Effects of observed horizontal inhomogeneities within cirrus clouds on solar radiative transfer. *Journal of Geophysical Research (Atmospheres)*, 107:4445, Oct. 2002.

Cahalan, R. F. and Snider, J. B. Marine stratocumulus structure. *Remote Sens. Environ.*, **95-107**:28, 1989.

Cahalan, R. F., Ridgway, W., Wiscombe, W. J., Bell, T. L., and Snider, J. B. The Albedo of Fractal Stratocumulus Clouds. *J ATMOS SCI*, **51** (16):2434–2455, aug 1994.

Cahalan, R. F., Silberstein, D., and Snider, J. B. Liquid Water Path and Plane-Parallel Albedo Bias during ASTEX. *Journal of Atmospheric Sciences*, **52**:3002–3012, Aug. 1995.

Carlin, B., Fu, Q., Lohmann, U., Mace, J., Sassen, K., and Comstock, J. M. High cloud horizontal inhomogeneity and solar albedo bias. *J. Climate*, **15**:2321–2339, 2002.

Choi, Y.-S. and Ho, C.-H. Radiative effect of cirrus with different optical properties over the tropics in MODIS and CERES observations. *Geophysical Research Letters*, **33**(21), 2006.

Cornet, C., C-Labonnote, L., and Szczap, F. Three-dimensional polarized Monte Carlo atmospheric radiative transfer model (3DMCPOL): 3D effects on polarized visible reflectances of a cirrus cloud. *J QUANT SPECTROSC RA*, jun 2010.

Corti, T. and Peter, T. A simple model for cloud radiative forcing. *Atmospheric Chemistry & Physics*, **9**:5751–5758, Aug. 2009.

Davies, R. The Effect of Finite Geometry on the Three-Dimensional Transfer of Solar Irradiance in Clouds. *Journal of Atmospheric Sciences*, **35**:1712–1725, Sept. 1978.

Davis, A., Marshak, A., Wiscombe, W., and Cahalan, R. Multifractal characterizations of nonstationarity and intermittency in geophysical fields: Observed, retrieved, or simulated. *Journal of Geophysical Research: Atmospheres*, **99**(D4):8055–8072, 1994.

Davis, A., Marshak, A., Wiscombe, W., and Cahalan, R. Scale Invariance of Liquid Water Distributions in Marine Stratocumulus. Part I: Spectral Properties and Stationarity Issues. *Journal of Atmospheric Sciences*, **53**:1538–1558, June 1996.

Davis, A., Marshak, A., Cahalan, R., and Wiscombe, W. The Landsat Scale Break in Stratocumulus as a Three-Dimensional Radiative Transfer Effect: Implications for Cloud Remote Sensing. *Journal of Atmospheric Sciences*, **54**:241–260, Jan. 1997.

Davis, A. B. and Marshak, A. Multiple scattering in clouds: Insights from three-dimensional diffusion/$P_1$ theory. *Nucl. Sci. Eng.*, **137**, 2001.

Dufresne, J.-L. and Bony, S. An Assessment of the Primary Sources of Spread of Global Warming Estimates from Coupled Atmosphere–Ocean Models. *Journal of Climate*, **21**(19):5135–5144, 2008.

Eguchi, N., Yokota, T., and Inoue, G. Characteristics of cirrus clouds from ICESat/GLAS observations. *GEOPHYS RES LETT*, **34**(9), 2007.

Fauchez, T., Cornet, C., Szczap, F., and Dubuisson, P. Assessment of cloud heterogeneities effects on brightness temperatures simulated with a 3D Monte-Carlo code in the thermal infrared. *International Radiation Symposium proceeding, Berlin, Germany*, page 4p., 2012.

Fauchez, T., Cornet, C., Szczap, F., Dubuisson, P., and Rosambert, T. Impacts of Cirrus Clouds Heterogeneities on TOA Thermal Infrared Radiation. *Atmospheric Chemistry and Physics*, 2014.

Fauchez, T., Dubuisson, P., Cornet, C., Szczap, F., Garnier, A., Pelon, J., and Meyer, K. Impacts of cloud heterogeneities on cirrus optical properties retrieved from space-based thermal infrared radiometry. *Atmospheric Measurement Techniques*, **8**(2):633–647, 2015.

Fauchez, T., Platnick, S., Meyer, K., Cornet, C., Szczap, F., and Várnai, T. Scale dependence of cirrus horizontal heterogeneity effects on TOA measurements – Part I: MODIS brightness temperatures in the thermal infrared. *Atmospheric Chemistry and Physics*, **17**(13):8489–8508, 2017a.

Fauchez, T., Platnick, S., Sourdeval, O., Meyer, K., Cornet, C., Zhang, Z., and Szczap, F. Cirrus heterogeneity effects on cloud optical properties retrieved with an optimal estimation method from MODIS VIS to TIR channels. *AIP Conference Proceedings*, **1810**(1): 040002, 2017b.

Forster, P., Ramaswamy, V., Artaxo, P., Berntsen, T., Betts, R., Fahey, D., Haywood, J., Lean, J., Lowe, D., Myhre, G., Nganga, J., Prinn, R., Raga, G., Schultz, M., and Van Dorland, R. Climate change 2007: The physical science basis. Contribution of Working Group I to the Fourth Assessment Report of the Intergovernmental Panel on Climate Change. *Cambridge University Press*, **44**:129–234, 2007.

Hartmann, D. L. and Short, D. A. On the use of earth radiation budget statistics for studies of clouds and climate. *Journal of Atmospheric Sciences*, **37**:1233–1250, June 1980.

Hogan, R. J. and Kew, S. F. A 3D stochastic cloud model for investigating the radiative properties of inhomogeneous cirrus clouds. *Q J ROY METEOR SOC*, **131**(611):2585–2608, 2005.

Jensen, E. J., Kinne, S., and Toon, O. B. Tropical cirrus cloud radiative forcing: Sensitivity studies. *Geophysical Research Letters*, **21**: 2023–2026, Sept. 1994.

Jensen, J. L. W. V. Sur les fonctions convexes et les inégalités entre les valeurs moyennes. *Acta Math.*, **30**:175–193, 1906.

Katagiri, S., Hayasaka, T., Shimizu, A., Matsui, I., Nishizawa, T., Sugimoto, N., and Takamura, T. Long term analysis of cirrus clouds: Effects on shortwave and longwave radiation derived from data acquired by ground-based and satellite-borne observations. *AIP Conference Proceedings*, **1531**(1):492–495, 2013.

Kato, S. and Marshak, A. Solar zenith and viewing geometry-dependent errors in satellite retrieved cloud optical thickness: Marine stratocumulus case. *Journal of Geophysical Research: Atmospheres*, **114**(D1), 2009.

Kobayashi, T. Effects Due to Cloud Geometry on Biases in the Albedo Derived from Radiance Measurements. *Journal of Climate*, **6**: 120–128, Jan. 1993.

L. H. Chambers, B. A. W. Independent Pixel and Two Dimensional Estimates of LANDSAT-Derived Cloud. Technical report, 1997.

Lane, D. E., Somerville, R. C. J., and Iacobellis, S. F. Sensitivity of cloud and radiation parameterizations to changes in vertical resolution. *jc*, **13**:915–922, 2000.

Liou, K. N. Influence of Cirrus Clouds on Weather and Climate Processes: A Global Perspective. *Monthly Weather Review*, **114**:1167, 1986.

Loeb, N. G. and Davies, R. Observational evidence of plane parallel model biases: Apparent dependence of cloud optical depth on solar zenith angle. *Journal of Geophysical Research*, **101**:1621–1634, Jan. 1996.

Lynch, D., Sassen, K., Starr, D., and Stephens, G. *Cirrus*. Oxford University Press, USA, 2002.

Marshak, A., Davis, A., Wiscombe, W., and Cahalan, R. Radiative smoothing in fractal clouds. *Journal of Geophysical Research*, **100**:26, 1995.

Marshak, A. and Davis, A. *3D radiative transfer in cloudy atmospheres*. Physics of Earth and Space Environments Series. Springer-Verlag Berlin Heidelberg, 2005.

Min, M., Wang, P., Campbell, J. R., Zong, X., and Li, Y. Midlatitude cirrus cloud radiative forcing over China. *J. Geophys. Res.*, **115** (D20210):75–99, 2010.

Minnis, P., Sun-Mack, S., Young, D., Heck, P., Garber, D., Chen, Y., Spangenberg, D., Arduini, R., Trepte, Q., Smith, W., Ayers, J., Gibson, S., Miller, W., Hong, G., Chakrapani, V., Takano, Y., Liou, K.-N., Xie, Y., and Yang, P. CERES Edition-2 Cloud Property Retrievals Using TRMM VIRS and Terra and Aqua MODIS Data x2014;Part I: Algorithms. *Geoscience and Remote Sensing, IEEE Transactions on*, **49** (11):4374–4400, Nov 2011.

Newman, W. I., Lew, J. K., Siscoe, G. L., and Fovell, R. G. Systematic effects of randomness in radiative transfer. *Journal of Atmospheric Sciences*, **52**:427–435, Feb. 1995.

Ohring, G. and Clapp, P. The Effect of Changes in Cloud Amount on the Net Radiation at the Top of the Atmosphere. *J ATMOS SCI*, **37**: 447–454, feb 1980.

Oreopoulos, L. and Cahalan, R. F. Cloud inhomogeneity from MODIS. *J. Climate*, **18**:5110–5124, 2005.

Oreopoulos, L. and Davis, R. Plane-parallel albedo bias from satellite observations. Part I: Dependence on resolution and other factorss. *J. Climate*, **11**:919–932, 1998.

Platnick, S. Approximations for horizontal photon transport in cloud remote sensing problems. *jqsrt*, **68**:75–99, Jan. 2001.

Platnick, S., Meyer, K. G., King, M. D., Wind, G., Amarasinghe, N., Marchant, B., Arnold, G. T., Zhang, Z., Hubanks, P. A., Holz, R. E., Yang, P., Ridgway, W. L., and Riedi, J. The MODIS Cloud Optical and Microphysical Products: Collection 6 Updates and Examples From Terra and Aqua. *IEEE Transactions on Geoscience and Remote Sensing*, **PP**(99):1–24, 2017.

Pujol, O. Comment on the (misused) concept of photon in radiative transfer, and proposition of a neologism. *JQSRT*, **159**:29–31, July 2015.

Ramanathan, V., Cess, R. D., Harrison, E. F., Minnis, P., Barkstrom, B. R., Ahmad, E., and Hartmann, D. Cloud-radiative forcing and climate: Results from the earth radiation budget experiment. *Science*, **243**(4887):57–63, 1989.

Rodgers, C. D. *Inverse Methods for Atmospheric Sounding Theory and Practice* . World Scientific, 2000.

Sassen, K., Wang, Z., and D., L. Global distribution of cirrus clouds from CloudSat/Cloud-Aerosol Lidar and Infrared Pathfinder Satellite Observations (CALIPSO) measurements. *J GEOPHYS RES-ATMOS*, **113**(D8), 2008.

Schmidt, K. S., Pilewskie, P., King, M. D., Wind, G., Tian, L., Platnick, S., and Arnold, T. Apparent absorption of solar radiation in heterogeneous tropical cirrus clouds. **11**:6578, Apr. 2009.

Stephens, G. L. Cloud Feedbacks in the Climate System: A Critical Review. *J CLIMATE*, **18**:237–273, Jan. 2005.

Stephens, G. L., Gabriel, P. M., and Tsay, S. Statistical radiative transport in one-dimensional media and its application to the terrestrial atmosphere. *Transport Theory and Statistical Physics*, **20**(2-3):139–175, 1991.

Szczap, F., Gour, Y., Fauchez, T., Cornet, C., Faure, T., Joudan, O., and Dubuisson, P. 3DCloud, a fast and flexible 3D cloud optical depth generator based on drastically simplified basic atmospheric equations and Fourier transform framework. Applications to stratocumulus, cumulus and cirrus cloud fields. *Geoscience Model Developpement*, **7**(1):1779–1801, 2014.

Várnai, T. and Davies, R. Effects of Cloud Heterogeneities on Shortwave Radiation: Comparison of Cloud-Top Variability and Internal Heterogeneity. *J ATMOS SCI*, **56**:4206–4224, Dec. 1999.

Varnai, T. and Marshak, A. Statistical analysis of the uncertainties in cloud optical depth retrievals caused by three-dimensional radiative effects. *J ATMOS SCI*, **58**(12):1540–1548, 2001.

Varnai, T. and Marshak, A. A method for analyzing how various parts of clouds influence each other's brightness. *Journal of Geophysical Research: Atmospheres*, **108**(D22), 2003.

Wendling, P. Albedo and Reflected Radiance of Horizontally Inhomogeneous Clouds. *Journal of Atmospheric Sciences*, **34**:642–650, Apr. 1977.

Yang, P., Bi, L., Baum, B., Liou, K.-N., Kattawar, G., Mishchenko, M., and Cole, B. Spectrally consistent scattering, absorption, and polarization properties of atmospheric ice crystals at wavelengths from 0.2 to 100 um. *J. Atmos. Sci.*, **70**:330–347, 2013.

Zhang, Z. and Platnick, S. An assessment of differences between cloud effective particle radius retrievals for marine water clouds from three MODIS spectral bands. *Journal of Geophysical Research: Atmospheres*, **116**(D20), 2011.

Zhang, Z., Platnick, S., Yang, P., Heidinger, A. K., and Comstock, J. M. Effects of ice particle size vertical inhomogeneity on the passive remote sensing of ice clouds. *Journal of Geophysical Research: Atmospheres*, **115**(D17), 2010. D17203.

Zhang, Z., Ackerman, A. S., Feingold, G., Platnick, S., Pincus, R., and Xue, H. Effects of cloud horizontal inhomogeneity and drizzle on remote sensing of cloud droplet effective radius: Case studies based on large-eddy simulations. *Journal of Geophysical Research: Atmospheres*, **117**(D19), 2012. D19208.

Zhang, Z., Werner, F., Cho, H.-M., Wind, G., Platnick, S., Ackerman, A. S., Di Girolamo, L., Marshak, A., and Meyer, K. A framework based on 2-D Taylor expansion for quantifying the impacts of subpixel reflectance variance and covariance on cloud optical thickness and effective radius retrievals based on the bispectral method. *Journal of Geophysical Research: Atmospheres*, **121**(12):7007–7025, 2016. 2016JD024837.

Zinner, T. and Mayer, B. Remote sensing of stratocumulus clouds: Uncertainties and biases due to inhomogeneity. *J GEOPHYS RES*, **111**: D14209+, July 2006.

Zinner, T., Wind, G., Platnick, S., and Ackerman, A. S. Testing remote sensing on artificial observations: impact of drizzle and 3D cloud structure on effective radius retrievals. *Atmospheric Chemistry and Physics*, **10**(19):9535–9549, 2010.

Zuidema, P. and Evans, K. F. On the validity of the independent pixel approximation for boundary layer clouds observed during ASTEX. *J. geophys. Res.*, **103**:6059–6074, Mar. 1998.

## Figures

Atmos. Chem. Phys. Discuss., https://doi.org/10.5194/acp-2018-38
Manuscript under review for journal Atmos. Chem. Phys.
Discussion started: 6 February 2018


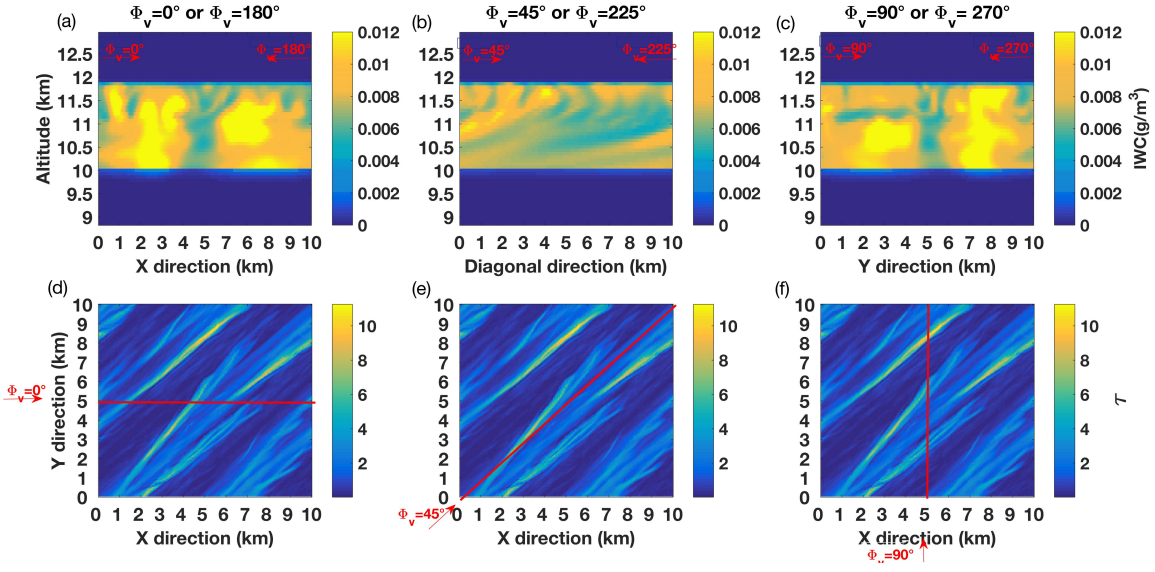


**Figure 1.** Top panels ((a), (b) and (c)) vertical distribution of the ice water content (IWC $(g/m^3)$) following the red line of the optical thickness field of bottoms panels ((d), (e) and (e)) along the red line as a function of the azimuth viewing angle $\Phi_v$.)

Atmos. Chem. Phys. Discuss., https://doi.org/10.5194/acp-2018-38
Manuscript under review for journal Atmos. Chem. Phys.
Discussion started: 6 February 2018


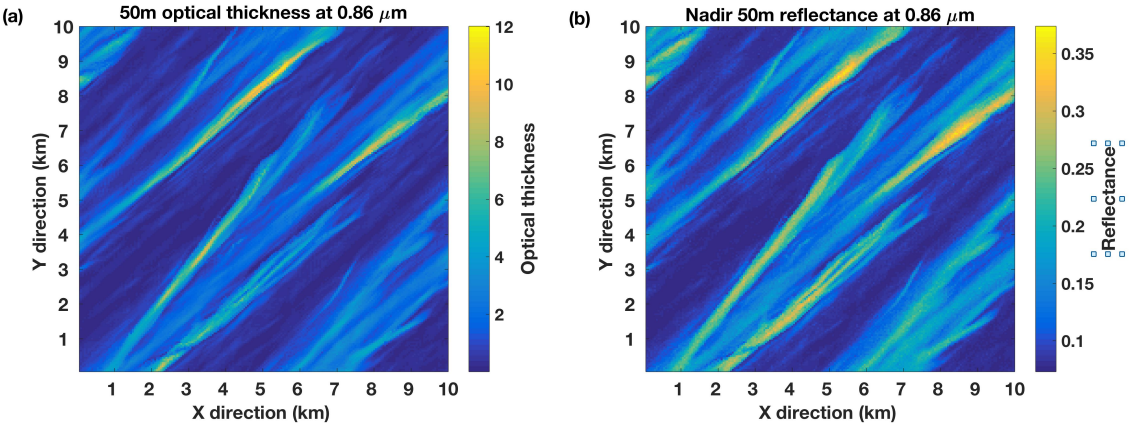


**Figure 2.** (a) Optical thickness field at 0.86 $\mu m$ and (b) solar reflectance field at 0.86 $\mu m$ at a spatial resolution of 50 m, with nadir view and overhead Sun.

Atmos. Chem. Phys. Discuss., https://doi.org/10.5194/acp-2018-38
Manuscript under review for journal Atmos. Chem. Phys.
Discussion started: 6 February 2018


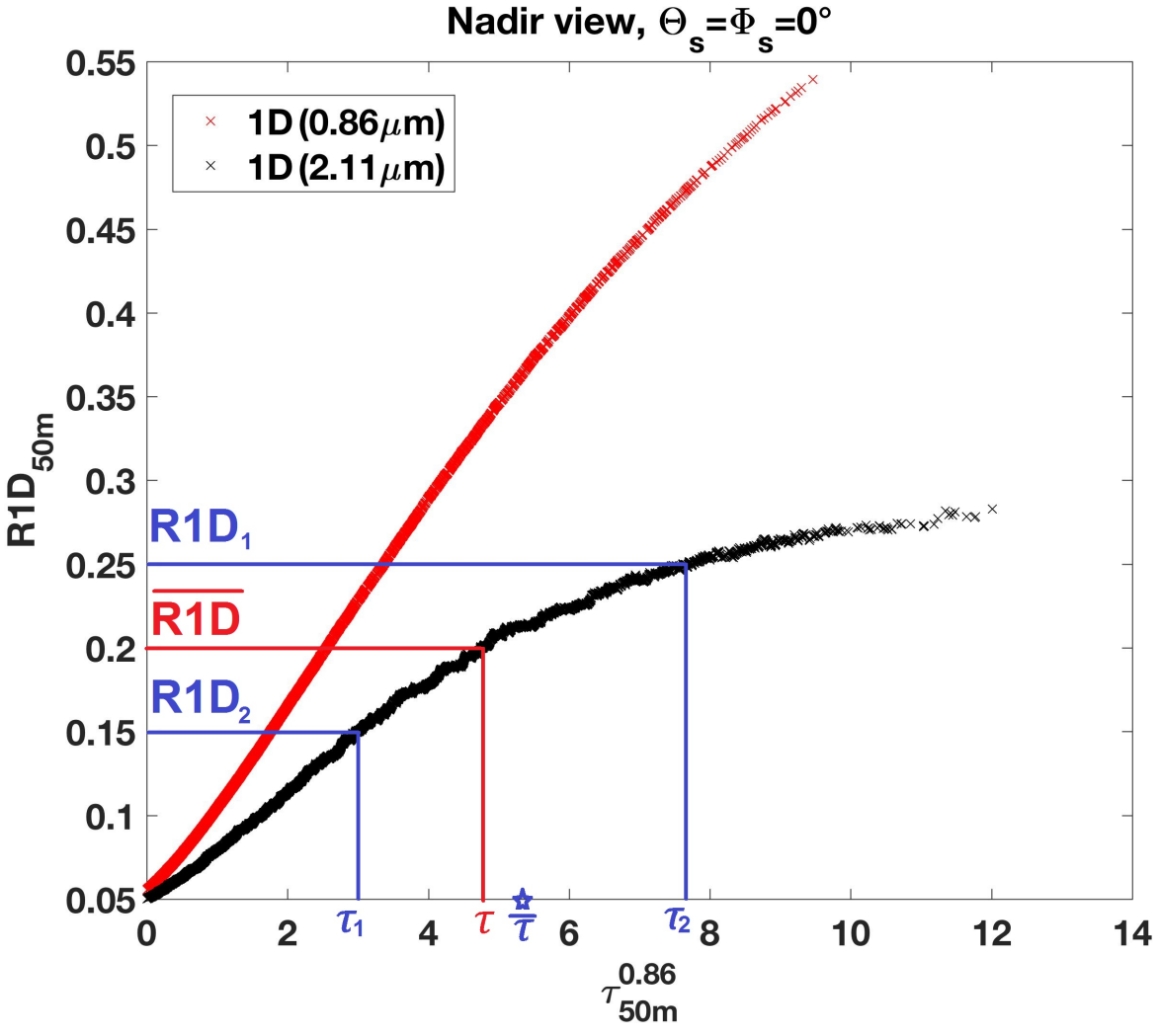


**Figure 3.** 1D reflectances ($R_{50m}$) as a function of the 50 m optical thickness at 0.86 $\mu m$ ($\tau_{50m}^{0.86\mu m}$) for channels centered at 0.86 $\mu m$ (red) and 2.13 $\mu m$ (black) for nadir view and overhead Sun. $\overline{R1D}$ represents the averaged of the two 2.13 $\mu m$ reflectances between reflectances $R1D_1$ and $R1D_2$ for which the optical thickness are $\tau_1$ and $\tau_2$, respectively, and $\bar{\tau}$ their averaged value. $\tau$ is the optical thickness associated with $\overline{R1D}$

Atmos. Chem. Phys. Discuss., https://doi.org/10.5194/acp-2018-38
Manuscript under review for journal Atmos. Chem. Phys.
Discussion started: 6 February 2018


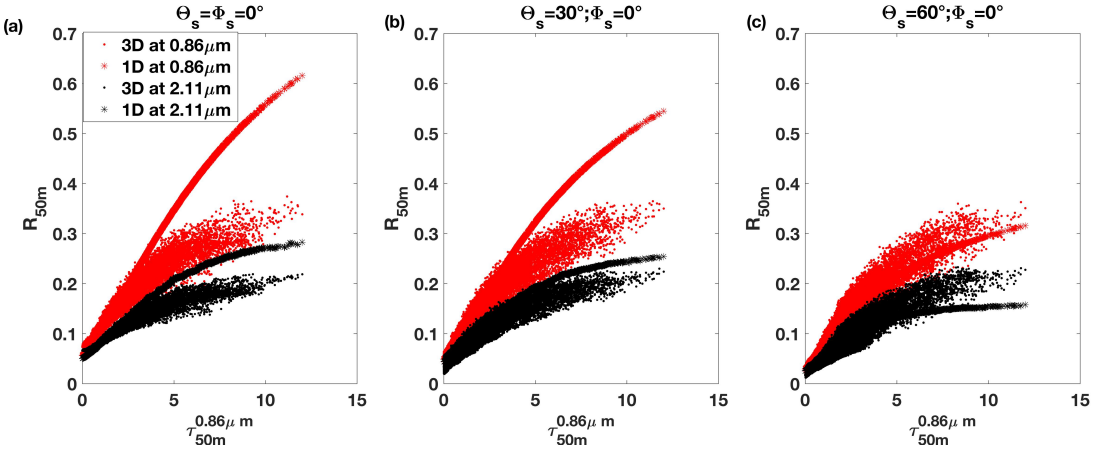


**Figure 4.** Reflectances ($R_{50m}$) for nadir view, as a function of the solar zenith angle $\Theta_s$ and 50 m optical thickness, at 0.86 $\mu m$ ($\tau_{50m}^{0.86\mu m}$) for channels centered at 0.86 $\mu m$ (in red color with 3D and 1D computations representing by star and dot markers, respectively) and 2.13 $\mu m$ (in black color with 3D and 1D computations representing by star and dot markers, respectively) and as function of the solar zenith angles $\Theta_s$.

Atmos. Chem. Phys. Discuss., https://doi.org/10.5194/acp-2018-38
Manuscript under review for journal Atmos. Chem. Phys.
Discussion started: 6 February 2018


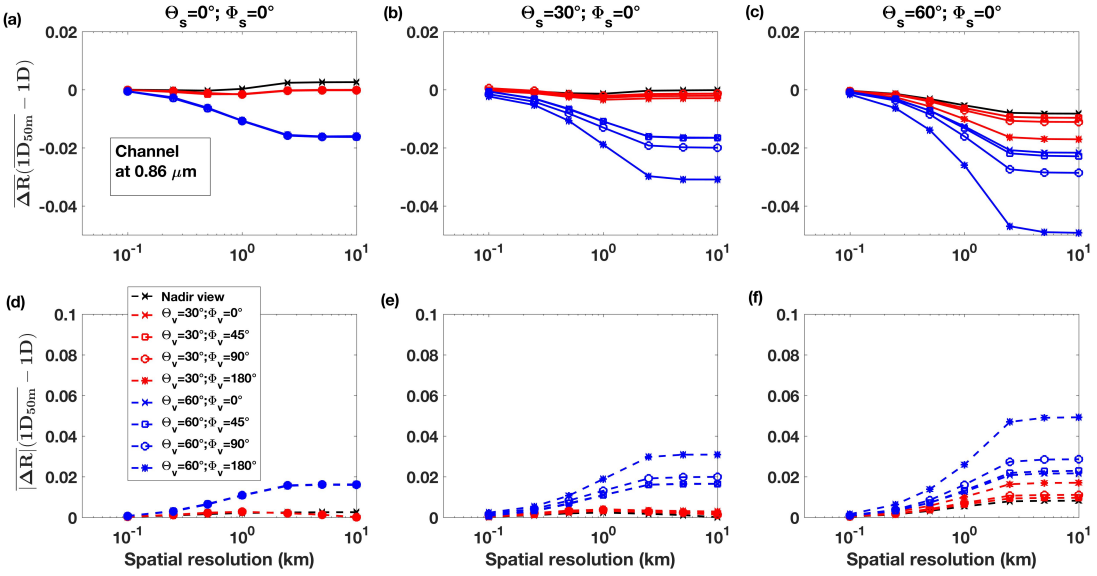


**Figure 5.** Arithmetic ($\overline{\Delta R}$) and absolute ($\overline{|\Delta R|}$) differences between 1D reflectances at $0.86\ \mu m$ estimated with Eq. 1 as a function of the spatial resolution for various view zenith and azimuth angles $\Theta_v$ and $\Phi_v$, respectively, and solar zenith angles $\Theta_s$.

Atmos. Chem. Phys. Discuss., https://doi.org/10.5194/acp-2018-38
Manuscript under review for journal Atmos. Chem. Phys.
Discussion started: 6 February 2018


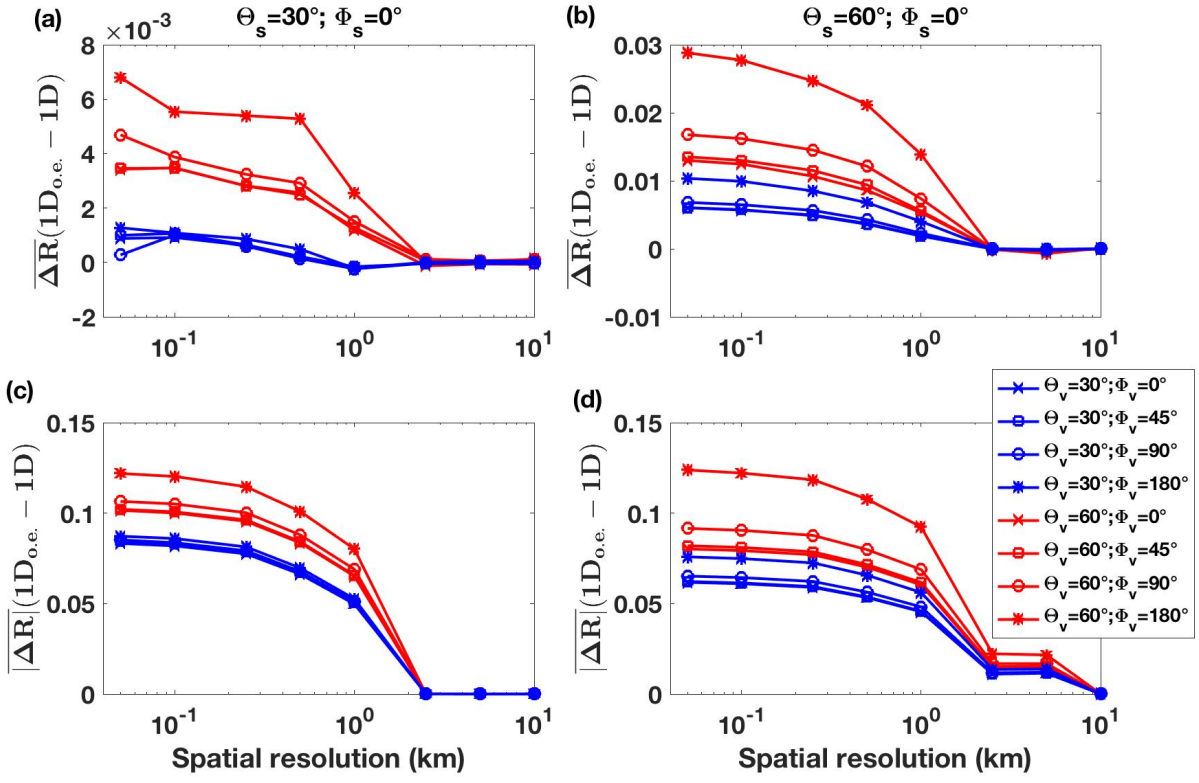


**Figure 6.** Tilted and homogeneous extinction approximation bias (THEAB) estimated with equations 2 (panels (a) and (b)) and 3 (panels (c) and (d)) for solar zenith angles of $\Theta_s = 30^\circ$ and $\Theta_s = 30^\circ$ and null solar azimuth angle, as a function of view zenith and azimuth angles $\Theta_v$ and $\Phi_v$.

Atmos. Chem. Phys. Discuss., https://doi.org/10.5194/acp-2018-38
Manuscript under review for journal Atmos. Chem. Phys.
Discussion started: 6 February 2018


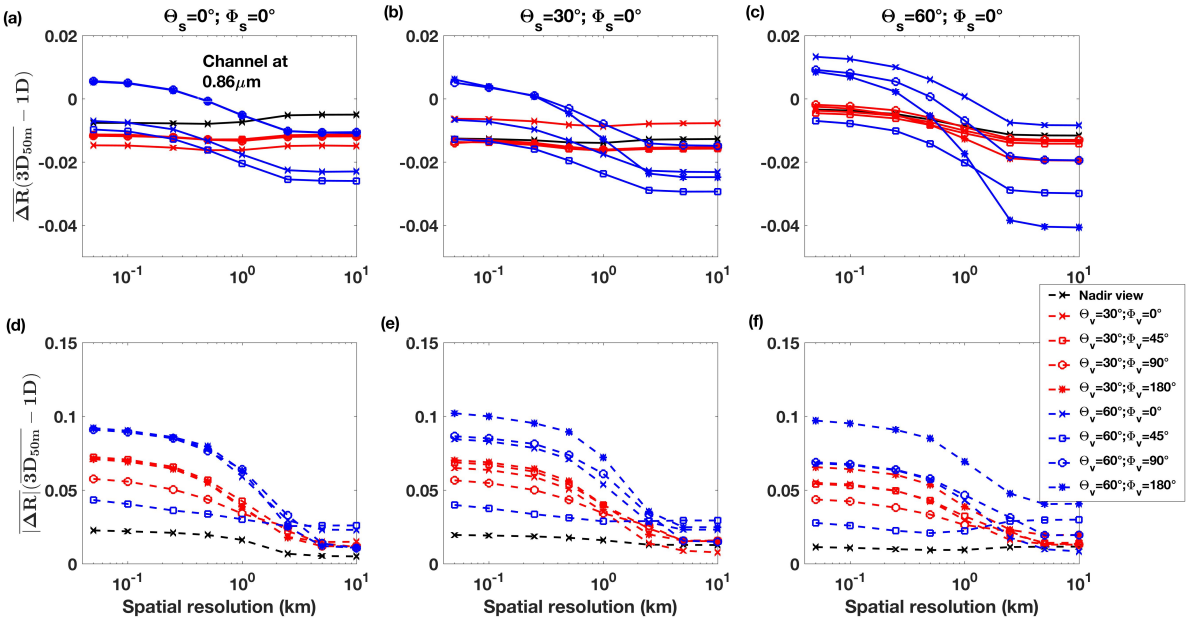


**Figure 7.** Arithmetic ($\overline{\Delta R}$) and absolute ($\overline{|\Delta R|}$) differences between 3D and 1D reflectances at 0.86 $\mu m$ estimated with equations 4 (panel (a), (b) and (c)) and 5 (panel (d), (e) and (f)), respectively, as a function of the spatial resolution, the view zenith and azimuth angles $\Theta_v$ and $\Phi_v$, respectively, and as a function of the solar zenith angles $\Theta_s$.

Atmos. Chem. Phys. Discuss., https://doi.org/10.5194/acp-2018-38
Manuscript under review for journal Atmos. Chem. Phys.
Discussion started: 6 February 2018


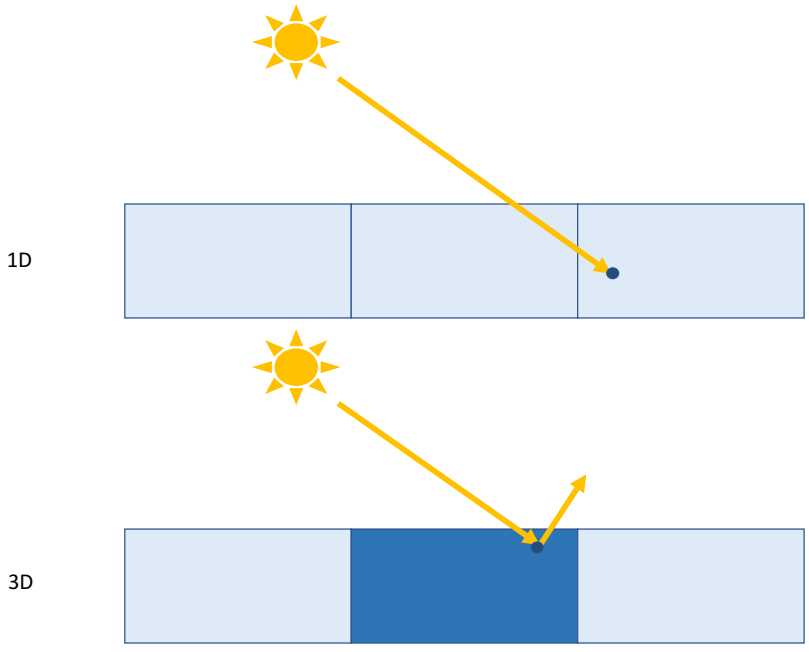


**Figure 8.** Illustration of the side illumination effect. In 1D (top panel) the right column can be highlighted by the photon coming from the Sun while in 3D (bottom panel), a thick neighbor region intercept first the photon and scatted it back to space, increasing the reflectance of the thick region, but reducing the reflectance of the thin region.

Atmos. Chem. Phys. Discuss., https://doi.org/10.5194/acp-2018-38
Manuscript under review for journal Atmos. Chem. Phys.
Discussion started: 6 February 2018


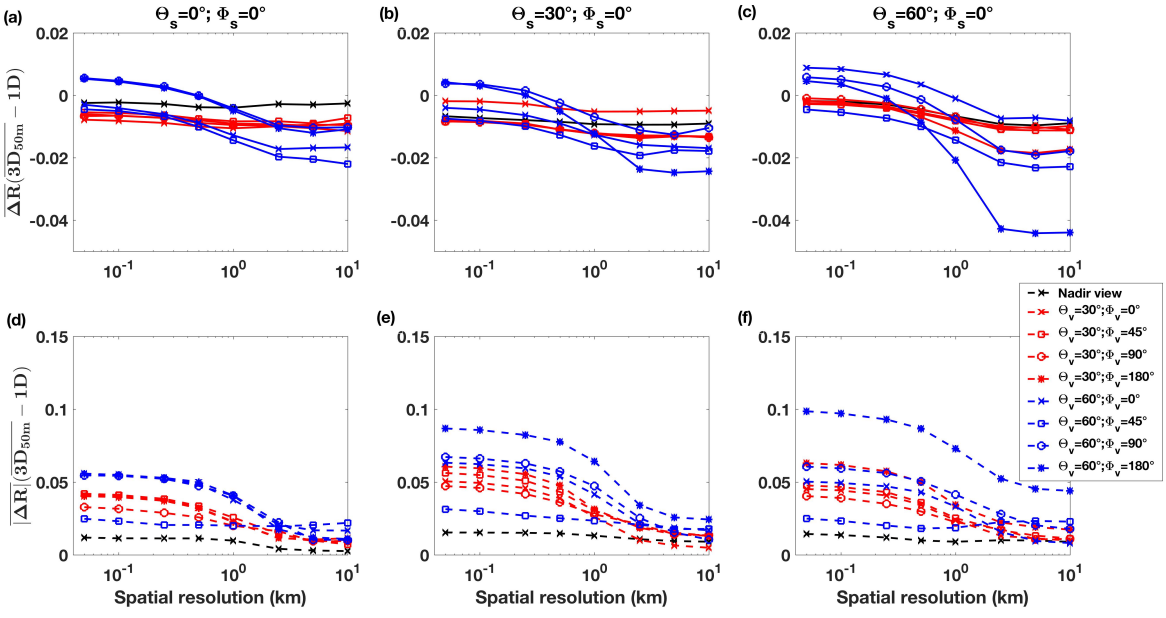


**Figure 9.** Arithmetic ($\overline{\Delta R}$) and absolute ($\overline{|\Delta R|}$) differences between 3D and 1D reflectances at 2.13 $\mu m$ estimated with equations 4 (panel (a), (b) and (c)) and 5 (panel (d), (e) and (f)), respectively, as a function of the spatial resolution, the view zenith and azimuth angles $\Theta_v$ and $\Phi_v$, respectively, and as a function of the solar zenith angles $\Theta_s$.

Atmos. Chem. Phys. Discuss., https://doi.org/10.5194/acp-2018-38
Manuscript under review for journal Atmos. Chem. Phys.
Discussion started: 6 February 2018


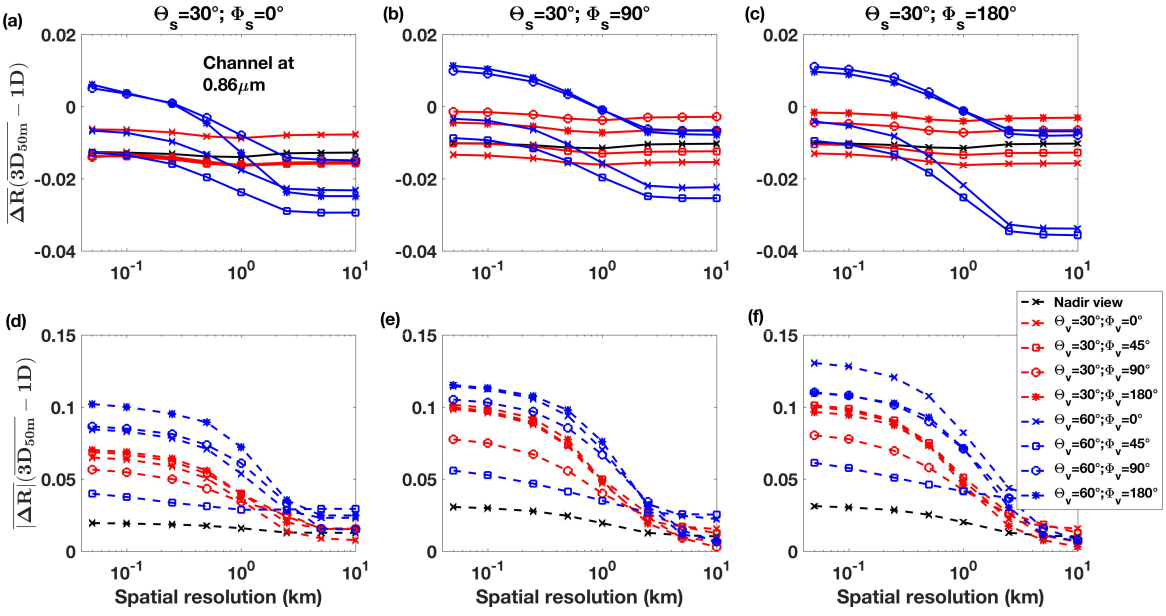


**Figure 10.** Arithmetic ($\overline{\Delta R}$) and absolute ($\overline{|\Delta R|}$) differences between 3D reflectances at $0.86\ \mu m$ estimated with equations 4 (panel (a), (b) and (c)) and 5 (panel (d), (e) and (f)), respectively, as a function of the spatial resolution, the view zenith and azimuth angles $\Theta_v$ and $\Phi_v$, respectively, and as a function of the solar azimuth angles $\Phi_s$ for solar zenith angle $\Theta_s = 30°$.

Atmos. Chem. Phys. Discuss., https://doi.org/10.5194/acp-2018-38
Manuscript under review for journal Atmos. Chem. Phys.
Discussion started: 6 February 2018


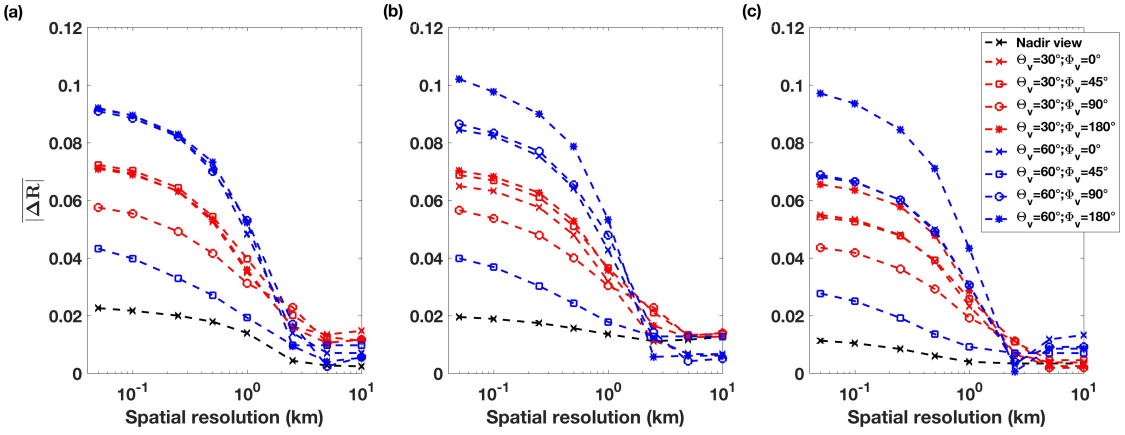


**Figure 11.** Absolute value of 3D effects averaged at each spatial resolution ($\overline{3D\ effects}$) at 0.86 $\mu m$ as a function of the view zenith and azimuth angles $\Theta_v$ and $\Phi_v$, respectively, and as a function of the solar zenith angles $\Theta_s$.

## Tables

Atmos. Chem. Phys. Discuss., https://doi.org/10.5194/acp-2018-38
Manuscript under review for journal Atmos. Chem. Phys.
Discussion started: 6 February 2018


Atmospheric Chemistry and Physics Discussions

**Table 1.** MOD06 optical properties of the ice crystal with an effective diameter of 20 $\mu m$ and an aggregate column shape provided by the Yang et al. (2013) model for the four channels use in this study.

| | $\sigma_e$ | $\varpi_0$ | g |
|---|---|---|---|
| MODIS channel 2 ($0.83\ \mu m$ ) | 2.085544 | 0.9999855 | 0.7526803 |
| MODIS channel 7 ($2.13 \mu m$ ) | 2.100113 | 0.9621367 | 0.7898260 |